Oxide Film Rupture, Reanodization, and Stress Corrosion Cracking in Aluminum

D. R. Arnott,[1] W. J. Baxter, and S. R. Rouze

General Motors Research Laboratories, Physics Department, Warren, Michigan 48090-9055

ABSTRACT

Several models have been proposed to account for the phenomenon of stress corrosion cracking (SCC), with varying emphasis on the roles of oxide film rupture, the rate of reoxidation, the segregation of alloying elements to grain boundaries, and embrittlement by hydrogen. This paper describes an investigation of thin anodic oxide films on 7075 aluminum with different levels of susceptibility to SCC. Photoelectron microscopy shows that during tensile deformation these oxide films develop microcracks along the grain boundaries, while measurements of the reanodization kinetics of similarly deformed specimens show that the rate of reanodization depends on the alloy composition and heat-treatment condition. For example, overaging of 7075-T6 aluminum produces subtle changes in the grain boundary chemistry, which increase the strength of the surface oxide film but slow down the process of reanodization. Results obtained from 7075 aluminum in three different heat-treatment conditions, and from 6061-T6 aluminum, show that the rate of reanodization consistently correlates with the susceptibility to SCC. This relationship offers a new and rapid method of assessing the vulnerability of these alloys to SCC.

Stress corrosion cracking (SCC) of the 7000 series of high strength aluminum alloys in chloride ion environments is due to the formation and growth of cracks of an almost brittle nature, which propagate along the grain boundaries. A number of mechanisms have been proposed (1) to account for the phenomenon, but as yet no consensus has emerged and it appears likely that several factors may be involved to varying degrees, depending on the particular circumstances. The problem is one of understanding the very localized nature of the cracking produced by the combination of a tensile stress and a chemically aggressive environment. Two of the proposed mechanisms which have received wide attention are the film rupture model (2-6) and the pre-existing active path model (7, 8), but neither provide a completely satisfactory explanation of the phenomenon. More recently attention has been focused on the role of hydrogen (9, 10), but much of the evidence has been obtained under conditions designed to promote hydrogenation rather than in an aqueous chloride environment.

In the pre-existing path model emphasis is placed on the microstructural and electrochemical parameters. Chemical inhomogeneities in the material are regarded as being the key factor. An example often quoted is the segregation of alloying elements in the form of precipitates at grain boundaries in 7075 aluminum, creating a precipitate-free zone (~50 nm wide), in the adjacent material. In a corrosive environment a highly localized electrochemical reaction can be established between the precipitates and the adjacent material. However, while this is an adequate explanation for intergranular corrosion, it does not account for the important role of tensile stresses in producing SCC.

According to the film rupture model the role of the tensile stress is to rupture the protective or passivating oxide film. This exposes highly localized regions of fresh metal surfaces with electrochemical potentials quite different from the surrounding areas still protected by the oxide film. Thus corrosion is envisaged to occur at these sites until a new passivating oxide film can reform. This fresh film will in turn be ruptured and the corrosion and repassivation processes repeated, thereby generating an active path for an SCC. However, it is argued that SCC will only occur if the repassivation kinetics are appropriate. If repassivation is very rapid, insufficent corrosion will occur to promote SCC. On the other hand, if repassivation is very slow, corrosion will be extensive rather than localized, and pitting, rather than SCC, will occur. Scully (6) has extended this model even further and proposed that SCC will only occur if, during repassivation, sufficient charge is passed to promote crack growth by anodic dissolution. This film rupture model has been criticized principally on the grounds that it does not account for the well-documented importance of microstructure. For example the susceptibility of 7075 aluminum to SCC is sensitive to heat-treatments which produce only very subtle microstructural changes (11). As such, this alloy is often cited in support of the pre-existing path model.

Evidence for the embrittling effect of hydrogen in aluminum alloys (9, 12) has invoked several mechanisms (10, 13, 14) where the focus for the action of hydrogen is at, or ahead of, the crack tip. However, the evidence is somewhat circumstantial as the conditions during SCC in a chloride environment differ appreciably from those often employed to investigate hydrogen effects (10, 15). Nevertheless if hydrogen is indeed the basis of the embrittlement during SCC, the kinetics may still be influenced, if not controlled, by such processes as hydrogen permeation (16) or stress-induced rupture of the oxide film.

This paper describes an investigation of 7075 aluminum that addresses the principal criticism of the oxide film rupture model, namely the influence of microstructural factors on the mechanical and electrochemical properties of the oxide film. Three different heat-treatment conditions of the alloy were investigated, and the stress corrosion susceptibility of each was measured in a chloride environment by the slow strain rate method (17). But recognizing the difficulties associated with a fundamental study of the passivating oxide films in such an environment, we chose instead, for purposes of analogy, to examine in detail the pertinent properties of thin (28 nm) anodic oxide films on those alloys. The rupture of these films was observed directly during tensile deformation in a photoelectron microscope, while the repassivation kinetics were studied by reanodization after tensile deformation. The oxide films are shown to rupture only along the grain boundaries, due to preferential deformation in the precipitate-free zone, while both the extent of rupture and the reanodization kinetics depend on the heat-treatment of the alloy. For comparison purposes, similar experiments were also performed on 1100-0 and 6061-T6 aluminum, which are minimally susceptible to SCC. For all the alloys examined, the rate of reanodization is found to increase systematically with the susceptibility to SCC and is proposed as the basis

[1] Present address: Aeronautical Research Laboratories, Melbourne, Victoria, Australia.

Key words: 7075 aluminum, SCC, oxide film rupture, photoelectron microscopy, reanodization kinetics.

for a new and rapid method of assessing the SCC resistance of aluminum alloys.

Experimental

Specimen preparation.—The specimens of 7075 aluminum were cut from a sheet of commercial alloy in the T6 temper, 1.5 mm thick and in the as-received condition. This material, which is rated as being moderately susceptible to SCC (18), was analyzed and found to contain by weight 6.4% Zn, 2.5% Mg, 1.7% Cu, 0.3% Fe, 0.2% Cr, and 0.1% Si. Most of the specimens were cut such that the applied tensile stress was perpendicular to the rolling direction of the sheet, the so-called L-T orientation, which is not the most susceptible orientation for this material. (Most investigators cut their samples with the tensile axis parallel to the thickness of plate material thereby taking advantage of the anisotropic grain morphology to obtain the maximum degree of susceptibility to SCC.) Some specimens were also cut with the tensile axis parallel to the rolling direction, and these yielded very similar results.

Some of the samples were heat-treated to change the SCC susceptibility. To increase the susceptibility, the specimens were heated to 460°C for 1 hr and slowly cooled in air at 4°C/sec, followed by aging at 120°C for 24 hr. This treatment is known to produce precipitates both within the grains and in the grain boundaries, which are considerably larger than those existing in the quenched and tempered T-6 condition (19). To decrease the susceptibility the T-6 material was overaged at 160°C for 24 hr to convert it to the T-7 condition. For comparison purposes a few specimens of 1100-0 and 6061-T6 aluminum were included as representative of materials which are minimally susceptible to SCC.

Constant strain rate tests.—The susceptibility to SCC was measured in a chloride ion environment by the slow strain rate technique (17). Conventional parallel-sided tensile specimens, with a gauge section 14 mm wide and 75 mm long, were deformed in an Instron machine at strain rates $\geq 9 \times 10^{-7}$. These specimens received no special surface preparation other than a thorough degreasing with acetone. During tensile deformation the specimens were surrounded by a plexiglass jacket containing 1*N* $AlCl_3$ solution, aerated by a continuous flow of air bubbles [this solution has been used by Maitra for similar tests on the 2××× series of aluminum alloys (20)]. This solution was selected because it is inherently more aggressive than a 1*N* NaCl solution, a fact that was borne out by preliminary static load tests on the 7075-T6 alloy.

Anodic film formation.—The thin (28 nm) oxide films were formed by anodization in a solution of 3% tartaric acid, adjusted to $pH = 5$ with NH_4OH. Prior to anodization, these specimens were degreased with acetone and cleaned further by immersion in chromic acid at 70°C for 10 min. To obtain oxides of controlled thickness, the current density during anodization was limited to ~1 mA/cm² by increasing the applied voltage slowly until 20V was attained. The current was then allowed to decay for a period of 10 min at a constant 20V. This procedure produces reproducible oxide films of low defect density (21).

Oxide film rupture.—The development of microcracks in these anodic oxide films during tensile deformation was studied by two techniques.

1. The extent and mode of fracture was observed directly during tensile deformation of small samples in the photoelectron microscope. This microscope, which has been described previously (22), is very sensitive to surface effects and has the unique capability of imaging microcracks in very thin oxide films. The specimens are deformed by bending so that the surface under examination is subjected to known amounts of tensile strain.

2. The extent of fracture of the oxide was measured by the reanodization current transient method described previously (23). These experiments were conducted on parallel-sided tensile specimens, as used in the slow strain rate tests. After tensile deformation the microcracks produced in the 28 nm oxide (formed at +20V) were reanodized at a lower voltage (+10V), and the current transient recorded on a digital oscilloscope. In previous studies on 1100 aluminum, the time constant (τ) of this exponentially decaying current transient was shown to be proportional to the area of metal being reanodized, *i.e.*, the total area of the microcracks produced in the 28 nm oxide.

Results

Slow strain rate tests.—Since the slow strain rate technique has been developed only in recent years and has yet to win complete acceptance as a method of measuring SCC, a series of experiments were performed to establish that it provided a good comparative measure of the severity of SCC in our specimens. In these experiments the total elongation in tensile tests at low strain rates was found to be the most sensitive measure of SCC.

The effect of strain rate on the total elongation of 7075-T6 aluminum, deformed in aerated $AlCl_3$, is shown in Fig. 1. At low strain rates there is a marked reduction of ductility. This reduction of total elongation was accompanied by a disappearance of the load reduction normally associated with ductile necking, as well as the appearance of secondary cracking, demonstrating a fundamental change to a brittle mode of failure. It is anticipated that the curve in Fig. 1 would continue to even lower values of total elongation at lower strain rates, but such measurements usually require specially designed equipment. Nevertheless the trend is already well established, so the loss of ductility at a strain rate of 9×10^{-7} sec^{-1} was used as a measure of the susceptibility to SCC.

The slow strain rate procedure was conducted at a rate of 9×10^{-7} sec^{-1} on 6061-T6 aluminum and samples of 7075 aluminum that had been heat-treated in ways known to change the stress corrosion susceptibility. As described earlier, these consisted of a simple heat-treatment to increase the susceptibility and overaging to decrease the susceptibility. Since both these heat-treatments changed the inherent ductility of the material, it was also necessary for control purposes to test such specimens in air. The results obtained in the $AlCl_3$ solution are therefore expressed in terms of the loss of ductility (reduced elongation) with respect to those deformed in air. The summary in Table I shows that the ordering of susceptibility to SCC is in agreement with that generally accepted on the basis of the more conventional test procedures (19).

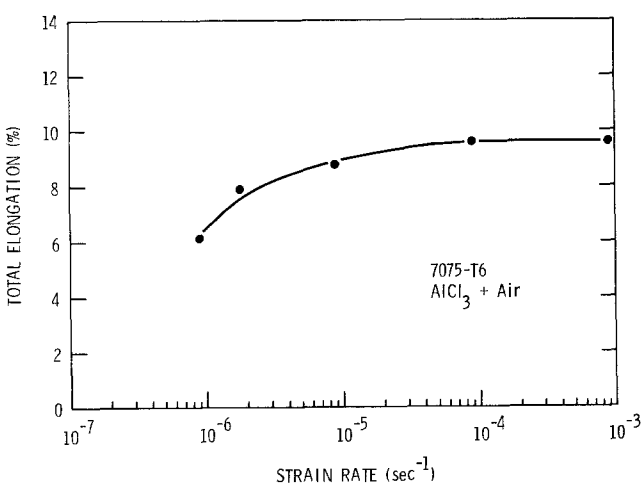

Fig. 1. Effect of strain rate on the total elongation of 7075-T6 aluminum deformed in aerated $AlCl_3$ at 20°C.

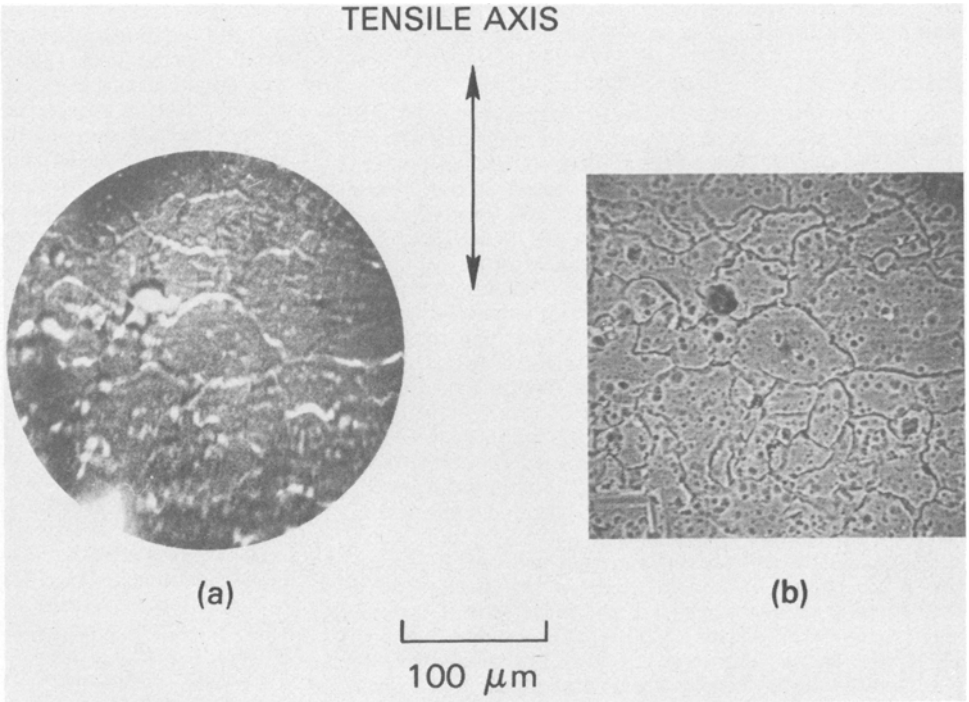

Fig. 2. (a) Photoelectron micrograph of 7075-T6 aluminum after a tensile strain of 4.5×10^{-2}. Sources of exoelectron emission (white regions) identify sites of rupture of 28 nm oxide film. (b) Scanning electron micrograph of same area showing grain structure.

Photoelectron microscopy of oxide rupture.—In the photoelectron microscope (PEM), the specimen is illuminated by u.v. light and the emitted photoelectrons form an image of the surface of the sample on a fluorescent screen. Any microcracks that develop in the surface oxide appear as regions of more intense photoelectron emission, often referred to as photostimulated exoelectron emission (24). Thus in the photoelectron micrographs shown below, the microcracks appear as white regions, in strong contrast with the areas covered by the intact oxide that emit relatively few electrons and appear black.

During tensile deformation of a specimen of 7075-T6 aluminum, the onset of exoelectron emission from microcracks in a 28 nm surface oxide occurs at a strain of 1×10^{-2}. More microcracks develop as the strain increases, as illustrated by the photoelectron micrograph in Fig. 2(a) that shows the numerous sources of exoelectron emission produced by a tensile strain of 4.5×10^{-2}. The relationship of these microcracks in the surface oxide to the underlying microstructure of the metal substrate is provided by comparison with the scanning electron micrograph of the same area in Fig. 2(b) ("sample current" image). It is evident that the microcracks develop primarily along the grain boundaries. A few cracks also develop around inclusions; in this regard it should be noted that the large inclusion in Fig. 2 is atypical. (The strong emission at the lower left of Fig. 2a originates from the corner of the scratch visible in Fig. 2b. This scratch was applied deliberately for identification purposes.)

This fracture mode of the oxide film on 7075-T6 aluminum is distinctly different from that observed during similar experiments on 1100-0 aluminum. The photoelectron micrograph in Fig. 3 shows the exoelectron emission from a specimen of 1100-0 aluminum after a tensile strain of 4.5×10^{-2}. In this case the microcracks in the 28 nm oxide are produced by the emergence of transgranular slip, as has been reported previously (25). Also the total area of microcracks in the oxide on 1100-0 aluminum was in general slightly larger than that in the oxide of 7075-T6 aluminum. (In similar experiments on 6061-T6 aluminum, the density of microcracks was observed to be very similar to that for 1100-0 aluminum.)

Quite different results were obtained from overaged 7075 aluminum. Three specimens were deformed in the PEM producing a tensile strain of 4.5×10^{-2}; two of these specimens developed only a single isolated small spot of exoelectron emission, while the third developed none at all. (In one experiment the specimen was fatigue cycled at this high strain level: 10 cycles produced several sites of exoelectron emission.) Thus the 28 nm oxide film on overaged 7075 aluminum is remarkably resistant to fracture.

Two heat-treated specimens were also deformed in the PEM. The results were similar to those for the T-6

Table I. Susceptibility of aluminum alloys as measured at strain rate of 9×10^{-7} sec^{-1} in $AlCl_3$ solution

Alloy	Loss of ductility (%)
7075 heat-treated*	56
7075 T-6	36
7075 T-7x	20
6061 T6	14

* To produce high degree of susceptibility, see text.

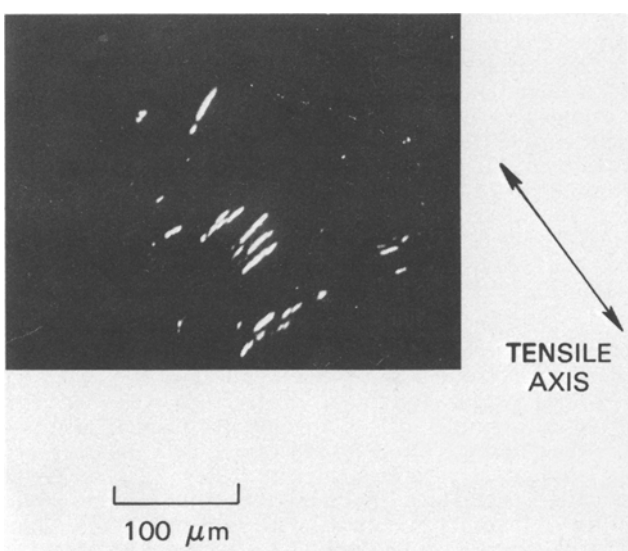

Fig. 3. Photoelectron micrograph of 1100-0 aluminum with 28 nm oxide after tensile strain of 4.5×10^{-2}.

temper, with clear evidence of oxide rupture at grain boundaries. However, the extent of rupture was not quite as great: after a tensile strain of 4.5×10^{-2} the density of microcracks was estimated to be approximately 60% of that observed for the T-6 condition (Fig. 2a).

The striking effect of overaging 7075 aluminum on the subsequent fracture resistance of the anodic oxide film prompted a more detailed examination by more conventional forms of electron microscopy. First, several of the specimens of 7075-T6 aluminum were transferred from the PEM to a scanning electron microscope to examine the sites of oxide rupture in more detail. But we were unable to find any topographical feature to distinguish these sites from other grain boundaries where no oxide rupture had occurred. However, in a series of separate experiments on well-polished specimens, which had not been cleaned in chromic acid and were coated with only the thin natural oxide, some of the exoelectron emitting grain boundaries showed evidence of localized plastic deformation. The scanning electron micrograph in Fig. 4 was obtained from a specimen deformed to a tensile strain of 7×10^{-2} and shows an array of fine slip lines along a grain boundary where oxide rupture had been observed in the PEM. Note that the deformation is confined to a region $\leq$ 100 nm wide, which is consistent with previous observations of preferential grain boundary deformation in these alloys (26).

Some specimens of T-6 and overaged 7075 aluminum were thinned for microstructural examination in a scanning transmission electron microscope. As details of this work have been reported elsewhere (27), it suffices here to describe only the salient results. First the width of the precipitate-free zone (PFZ) adjacent to grain boundaries was typically ~60 nm for both T6 and averaged material, which is consistent with previous observations (11, 26) and is comparable to the width of the deformed region in Fig. 4. Second, the T-6 and overaged material showed important differences in the grain boundary chemistry. Overaging of the T-6 structure promoted (*i*) coarsening of the Zn-, Cu- and Mg-rich grain boundary precipitates, (*ii*) the development at the grain boundaries of a previously undetected Si-rich precipitate, and (*iii*) the removal of Cu, Zn, and Si from the PFZ.

These changes in the grain boundary could be expected to soften the material in the PFZ and permit deformation to occur more easily in the overaged material. While this can account for the well-known reduction of strength by overaging, it does not readily account for the increased fracture resistance of the oxide. A possible explanation of the latter may lie in the control of oxide rupture by inherent defects in the oxide film (21). The material in the PFZ of overaged alloy is purer than that in the T-6 condition, so that an oxide film may be grown with fewer defects and a greater resistance to fracture.

Reanodization measurement of oxide rupture.—The oscilloscope traces of reanodization current transients shown in Fig. 5 are for a series of specimens of parallel-cut 7075 T-6 aluminum deformed in tension by different amounts. The bottom curve is for an undeformed specimen and shows the current flow required to charge up the capacitor formed by the metal substrate, oxide film, and electrolyte. This charging current is subtracted from the other curves to obtain the true reanodization currents, which decay exponentially with a well-defined time constant (τ). The existence of a reanodization current after a tensile strain of 1×10^{-2} is clear evidence of oxide film rupture, and the reanodization current increases substantially as the extent of rupture increases with increasing tensile strain. Thus these results are in complete accord with the observations by photoelectron microscopy.

Since the value of τ is proportional to the total area of metal being reanodized, it must be normalized with respect to the surface area (A) of the specimen to provide a measure of the density of microcracks. The effect of tensile strain on the measured values of τ/A is shown in Fig. 6 for 7075-T6 and 1100-0 aluminum. The value of τ/A increases with increasing deformation for both materials, but the values for the 7075 aluminum are much larger than those for 1100-0 aluminum. Since direct observation in the photoelectron microscope showed that for a given tensile strain the area of fresh metal surface exposed by oxide fracture was very similar for these two materials, we conclude that τ is also a function of the chemical composition of the material being anodized.

To investigate the effect of chemical composition on the anodization kinetics, the anodization current transients for known areas of freshly cleaned surfaces of 1100-0, 7075-T6, and 6061-T6 aluminum were determined. The measured values of the decay time constant per unit area (τ_1) for these three alloys are listed in Table II. The value for 7075-T6 aluminum is 70% larger than that for 1100-0 aluminum, but this is not sufficient to account for the difference between

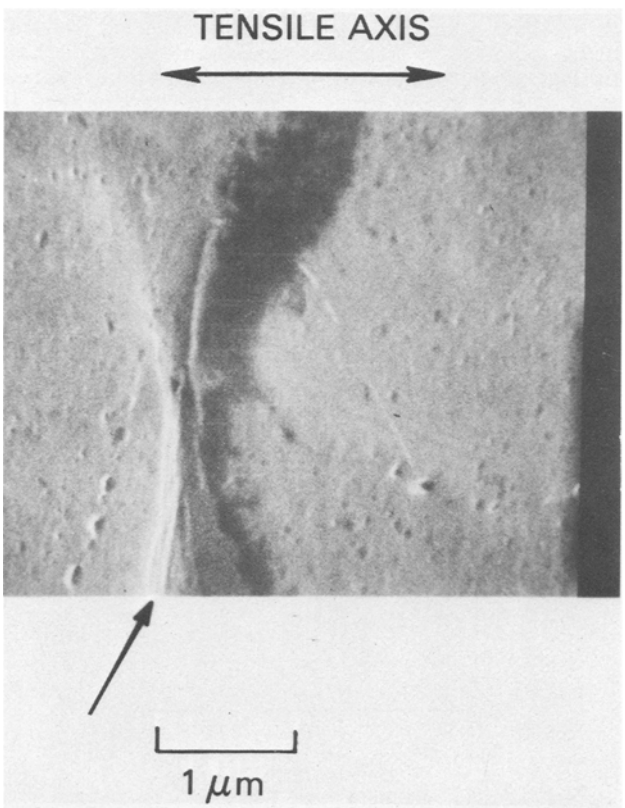

Fig. 4. Scanning electron micrograph of 7075-T6 aluminum. Arrow indicates slip deformation along a grain boundary at a location where oxide rupture had been observed in the PEM.

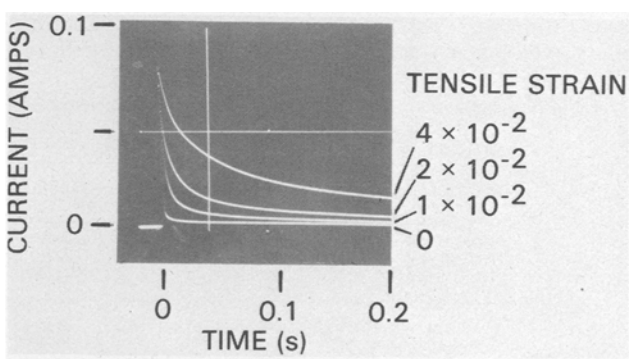

Fig. 5. Oscilloscope traces of the reanodization current transients to 7075-T6 aluminum after tensile deformation.

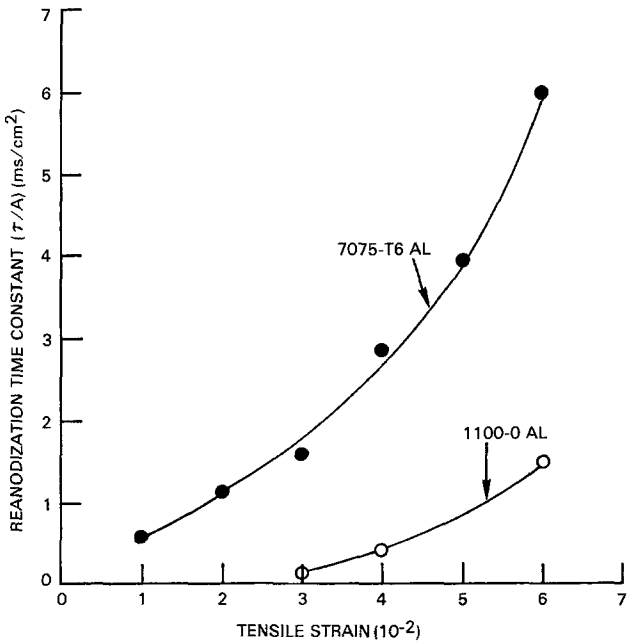

Fig. 6. Reanodization current time constant τ (normalized with respect to specimen surface area A) as a function of tensile strain for 7075-T6 and 1100-0 aluminum.

the two sets of results in Fig. 6. Also listed in Table II are the values of τ/A measured for the three alloys during reanodization after a tensile strain of 4×10^{-2}. Comparison of the data for 1100-0 and 7075-T6 aluminum with that for 6061-T6 aluminum reveals a similar discrepancy. In the final column of Table II are listed the calculated values of τ/A for reanodization after a tensile strain of 4×10^{-2}. These were calculated from the following equations

$$\tau/A = \tau_1 \frac{\Delta A}{A} \qquad [1]$$

where ΔA is the area of the microcracks and

$$\frac{\Delta A}{A} = 0.57\ (\epsilon_1 - \epsilon_0) \qquad [2]$$

where ϵ_1 is the tensile strain and $\epsilon_0 = 1 \times 10^{-2}$ is the observed value of strain required for the onset of oxide fracture. Equation [2] is derived on the basis of (a) constant specimen volume, *i.e.*

$$\epsilon_1 + \epsilon_2 + \epsilon_3 = 0$$

where ϵ_1, ϵ_2, and ϵ_3 are the strains in the three principal directions, and (b) the empirical relationship

$$\epsilon_2 = R\epsilon_3$$

where $R = 0.7$ for these alloys (28).

Comparison of the calculated and measured values of τ/A for all three alloys shows that these 28 nm oxide films are remarkably fracture resistant. Furthermore, comparison of the experimental values of τ/A with τ_1 shows that, when rupture does occur, the rate of reanodization is a strong function of the material revealed. For example, whereas the value of τ_1 for 7075-T6 aluminum is only 1.7 times that for 1100-0 aluminum, after tensile deformation the value of τ/A for 7075-T6 aluminum is 8.5 times that for 1100-0 aluminum. This is a clear indication that the chemical composition of the material revealed by the microcracks in the oxide film on 7075-T6 aluminum is not representative of the overall composition of the alloy. This is entirely consistent with the results of the previous section where it was shown that the oxide film ruptures preferentially along the grain boundaries, where there is pronounced segregation of the alloying elements. Thus the value of τ/A after tensile deformation is sensitive to not only the area, but also the composition, of the material exposed by the microcracks in the oxide film.

Table II. Anodization and reanodization current time constants for three aluminum alloys

Alloy	Initial anodization, τ_1 (msec/cm²)	Reanodization after tensile strain = 4×10^{-2}	
		Measured (τ/A) (msec/cm²)	Calculated (τ/A) (msec/cm²)
1100-0	310	0.4	5.3
6061-T6	350	1.25	6
7075-T6	530	3.4*	9

* See Fig. 7.

Correlation between SCC and reanodization kinetics. —The values of τ/A for reanodization after tensile deformation provide a very interesting comparison with our measurements of SCC susceptibility. A series of experiments were performed on the following alloys: 7075-T6, overaged and "poorly" heat-treated 7075 aluminum, and 6061-T6 aluminum. The values of τ/A were measured after a tensile strain of 4×10^{-2} and are plotted in Fig. 7 as a function of the loss of ductility measured in the slow strain rate tests. (A data point for 1100-0 aluminum would presumably lie near the origin since it is considered to be immune to SCC and has the small value of τ/A listed in Table II.) There is a remarkably simple correlation between the rate of reanodization and the susceptibility to SCC.

The explanation of this result is not entirely clear, but appears to be electrochemical in origin. For example, the experiments in the photoemission microscope showed that after a tensile strain of 4×10^{-2}, the area of microcracks in the oxide film on the overaged alloy was at least an order of magnitude smaller than those observed on the T-6 alloy. Yet the value of τ/A for the overaged material is ~70% of that for the T-6 alloy. Thus in this case the value of τ/A is being determined primarily by the composition of the material exposed by the microcracks in the oxide film. In fact, if the values of τ/A are further normalized with respect to the areas of microcracks observed in the PEM, then we estimate that the rate of reanodization per unit area of microcrack in the oxide film is

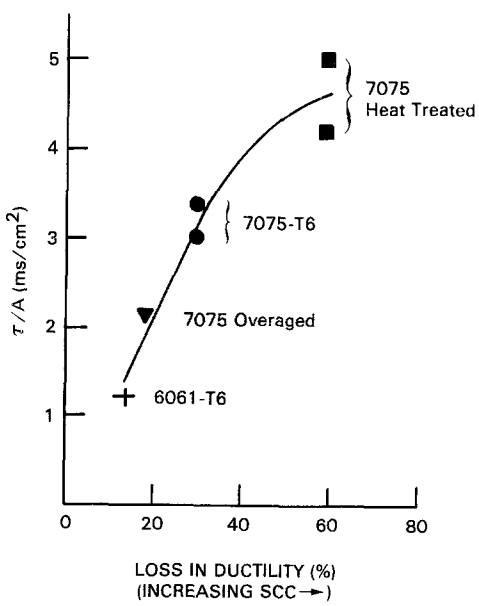

Fig. 7. Relationship between the loss of ductility measured from a slow strain rate SCC test and the reanodization current time constant (τ/A) measured after a tensile strain of 4×10^{-2}.

~30 times slower for the overaged material than for the T-6 alloy. (Similarly the rate for the heat-treated material is estimated to be twice as slow as for the T-6.)

It is tempting to anticipate that for these same conditions of the 7075 alloy, similar differences in both the rate of repassivation and the extent of rupture of the passivating film may occur in chloride solutions. If this is the case, then the observations presented here, of oxide rupture and reanodization, can be regarded as analogous to the events occurring during SCC, and a correlation of the type shown in Fig. 7 becomes reasonable.

Summary

During tensile deformation of 7075-T6 aluminum in a photoelectron microscope, surface oxide films were observed to fracture primarily along the grain boundaries. This was caused by deformation within the precipitate free zone, adjacent to the boundary (26). In a complementary series of measurements of reanodization current transients for deformed material, it was shown that the rate of reanodization of the microcracks in the oxide depends on both the alloy composition and heat-treatment condition. From these two sets of experiments we conclude that the measured rate of reanodization (τ/A) after deformation depends on both the area of the microcracks in the oxide and the chemical composition of the freshly exposed metal surfaces.

Microchemical analysis by scanning transmission electron microscopy shows that during overaging of 7075-T6 aluminum, increased precipitation occurs at the grain boundaries, removing Cu, Zn, and Si from the precipitate free zone. These subtle changes of chemistry appear to be responsible for two pronounced effects. First, the oxide film covering the grain boundary regions is much more fracture resistant on the overaged material than on the T-6 alloy. Second, when the oxide film does fracture, the material exposed on the overaged alloy reanodizes much more slowly than that on the T-6. It is these two influences of the area of microcracks and the composition of the exposed surfaces that result in the measured values of τ/A. These observations also suggest a new explanation of the well-known reduction of susceptibility to SCC by overaging 7075-T6 aluminum.

The correlation between the measured rate of reanodization (τ/A) after tensile deformation and the measured susceptibility to SCC, suggests that the phenomena of oxide rupture and reanodization kinetics are analogous to the film rupture and repassivation events that are believed to be important in SCC. In this regard we note that a similar correlation between SCC and passivation rates has been reported by Armstrong and Coates (29) for low carbon steel in carbonate/bicarbonate solution, a system that also produces intergranular fracture. However, their investigation differed from ours in that their passivation rates were measured for the entire surface of the alloy, rather than the specific regions of the grain boundary where oxide rupture occurred.

Finally, the correlation between the rate of reanodization and the susceptibility to SCC offers the basis of a novel test procedure for assessing the susceptibility of an alloy to SCC. Particularly noteworthy in this regard is the capability of distinguishing between the T6 and overaged condition of 7075 aluminum. Such a test offers a distinct advantage: it can be easily performed within ~20 min, whereas the slow strain rate test requires ~24 hr and the standard alternate immersion test for SCC occupies ~3 months.

Acknowledgments

The authors are grateful to A. Ottolini and T. P. Schreiber for the scanning electron micrographs. The authors also acknowledge constructive comments from the referee.

Manuscript submitted Aug. 3, 1981; revised manuscript received *ca.* March 24, 1982.

Any discussion of this paper will appear in a Discussion Section to be published in the June 1983 JOURNAL. All discussions for the June 1983 Discussion Section should be submitted by Feb. 1, 1983.

Publication costs of this article were assisted by General Motors Research Laboratories.

REFERENCES

1. R. N. Parkins, in "Corrosion," Vol. I, 8:3, L. L. Shreir, Editor, Newnes-Butterworths, Boston (1976).
2. H. L. Logan, *J. Res. NBS*, **48**, 99 (1952).
3. J. C. Scully, *Corros. Sci.*, **7**, 197 (1967).
4. T. J. Smith and R. W. Staehle, *Corrosion*, **23**, 117 (1967).
5. D. A. Vermilyea, *This Journal*, **119**, 405 (1972).
6. J. C. Scully, *Corros. Sci.*, **15**, 207 (1975).
7. E. H. Dix, *Trans. AIME*, **137**, 11 (1940).
8. R. N. Parkins, *Br. Corros. J.*, **7**, 15 (1972).
9. A. W. Thompson, *Mater. Sci. Eng.*, **43**, 41 (1980).
10. S. W. Ciaraldi, J. L. Nelson, R. A. Yeske, and E. N. Pugh, in "Hydrogen Effects in Metals," I. M. Bernstein and A. W. Thompson, Editors, p. 437, The Metallurgical Society, AIME (1981).
11. P. Doig, P. E. J. Flewitt, and J. W. Edington, *Corrosion*, **33**, 217 (1977).
12. M. O. Speidel, in "Hydrogen Effects in Metals," I. M. Bernstein and A. W. Thompson, Editors, p. 249, The Metallurgical Society, AIME (1981).
13. G. M. Scamans, R. Alani, and P. R. Swann, *Corros. Sci.*, **16**, 443 (1976).
14. S. P. Lynch, in "Hydrogen Effects in Metals," I. M. Bernstein and A. W. Thompson, Editors, p. 863, The Metallurgical Society, AIME (1981).
15. J. C. Scully, in "Environmental Degradation of Engineering Materials in Aggressive Environments," M. R. Louthan, R. P. McNitt, and R. D. Sisson, Editors, p. 143, Virginia Polytechnic Institute, Blacksburg, Virginia (1981).
16. R. Alani and P. R. Swann, *Br. Corros. J.*, **12**, 80 (1977).
17. "Stress Corrosion Cracking–The Slow Strain Rate Technique," ASTM STP 665 (1977).
18. See, B. F. Brown, "Stress Corrosion Cracking Control Measures," NBS (1977).
19. "Aluminum," Vol. I, ASM (1967).
20. S. Maitra, *Corrosion*, **37**, 99 (1981).
21. D. R. Arnott, W. J. Baxter, and S. R. Rouze, *This Journal*, **128**, 843 (1981).
22. W. J. Baxter and S. R. Rouze, *Rev. Sci. Instrum.*, **44**, 1628 (1973).
23. W. J. Baxter, *Met. Trans. A*, **11**, 1999 (1981).
24. W. J. Baxter, in "Research Techniques in Nondestructive Testing," Vol. 3, R. S. Sharpe, Editor, p. 395, Academic Press, London (1977).
25. W. J. Baxter and S. R. Rouze, *J. Appl. Phys.*, **44**, 4400 (1973).
26. A. J. Sedriks, P. W. Slattery, and E. N. Pugh, *Trans. ASM*, **62**, 238; 815 (1969).
27. B. V. N. Rao, *Met. Trans. A*, **12**, 1356 (1981).
28. S. S. Hecker, *Met. Eng. Quart.*, **14**, 30 (1974).
29. R. D. Armstrong and A. C. Coates, *Electrochim. Acta*, **21**, 79 (1976).